pH-Dependent Toxicity of High Aspect Ratio ZnO Nanowires in Macrophages Due to Intracellular Dissolution

Karin H. Müller,[†,‡] Jaideep Kulkarni,[‡] Michael Motskin,[†] Angela Goode,[‡] Peter Winship,[§] Jeremy N. Skepper,[†] Mary P. Ryan,[‡] and Alexandra E. Porter[‡,*]

[†]Multi-Imaging Centre, Department of Physiology, Development and Neuroscience/Anatomy Building, University of Cambridge, Downing Street, Cambridge CB3 2DY, United Kingdom, [‡]Department of Materials, Imperial College London, Exhibition Road, London SW7 2AZ, United Kingdom, and [§]MRC Human Nutrition Research, Elsie Widdowson Laboratory, Fulbourn Road, Cambridge CB1 9NL, United Kingdom

ABSTRACT High-aspect ratio ZnO nanowires have become one of the most promising products in the nanosciences within the past few years with a multitude of applications at the interface of optics and electronics. The interaction of zinc with cells and organisms is complex, with both deficiency and excess causing severe effects. The emerging significance of zinc for many cellular processes makes it imperative to investigate the biological safety of ZnO nanowires in order to guarantee their safe economic exploitation. In this study, ZnO nanowires were found to be toxic to human monocyte macrophages (HMMs) at similar concentrations as $ZnCl_2$. Confocal microscopy on live cells confirmed a rise in intracellular Zn^{2+} concentrations prior to cell death. *In vitro*, ZnO nanowires dissolved very rapidly in a simulated body fluid of lysosomal pH, whereas they were comparatively stable at extracellular pH. Bright-field transmission electron microscopy (TEM) showed a rapid macrophage uptake of ZnO nanowire aggregates by phagocytosis. Nanowire dissolution occurred within membrane-bound compartments, triggered by the acidic pH of the lysosomes. ZnO nanowire dissolution was confirmed by scanning electron microscopy/energy-dispersive X-ray spectrometry. Deposition of electron-dense material throughout the ZnO nanowire structures observed by TEM could indicate adsorption of cellular components onto the wires or localized zinc-induced protein precipitation. Our study demonstrates that ZnO nanowire toxicity in HMMs is due to pH-triggered, intracellular release of ionic Zn^{2+} rather than the high-aspect nature of the wires. Cell death had features of necrosis as well as apoptosis, with mitochondria displaying severe structural changes. The implications of these findings for the application of ZnO nanowires are discussed.

KEYWORDS: zinc oxide nanowires · macrophages · cytotoxicity · electron microscopy · dissolution morphology · biodegradation · simulated body fluid

Metal oxide nanowires are at the forefront of application driven nanotechnology research. They offer distinct advantages over their bulk counterparts in many applications ranging from transistors to sensors. ZnO is a direct bandgap semiconductor which has attracted a vast quantity of research owing to its wide range of optoelectronic and electrical properties, including transparency in the visible and high infrared reflectivity, piezoelectric effect, chemical, and thermal stability and its 'absence of toxicity' at least in bulk form.[1] In addition, it is easily doped to provide novel magnetic properties (such as dilute magnetic semiconducting behavior), and hence it has potential in spintronics. The special optoelectronic properties of ZnO nanowires are hugely important for the development of novel nanosensors, nanotransducers, photocatalysts, and nanogenerators.[1,2] Within the past few years, it has become one of the most important products in the nanosciences besides carbon and silicone nanomaterials.[3] For many of the proposed applications, the formation of one-dimensional (1D) ZnO nanostructures (*e.g.*, wires, rods, and tubes) offers an advantage over bulk material as many novel properties, such as enhanced photoluminescence and lasing, are being observed with the formation of engineered nanoscale high aspect ratio structures. While the functional properties of ZnO nanostructures are being exploited and developed, little is known regarding their toxicity. It is essential to address these issues before they are manufactured on a large scale and introduced into commercial products.

In biological systems, zinc is a multipurpose element. On the one hand, it is an essential trace element involved in a wide number of biological processes, such as metabolism, cell proliferation and differentiation, signal transduction, and control of gene expression.[4−6] It is a component of over 300 enzymes, as in either a catalytic or regulatory cofactor or a structural capacity.[4] It is therefore not surprising that severe zinc deficiency in humans can lead to a range of ailments, such as dermatitis, diarrhea, anorexia, neurosensory disorders, and cell-mediated immune dysfunction. The genetic disorder acrodermatitis enteropathica, which affects enteral zinc absorption,

*Address correspondence to a.porter@imperial.ac.uk.

Received for review May 28, 2010 and accepted September 30, 2010.

Published online October 15, 2010. 10.1021/nn101192z

can be fatal if left untreated.[7] Oral zinc supplementation has proven beneficial in a number of infectious diseases, particularly in acute lower respiratory infections, leprosy, diarrhea, and tuberculosis,[6] and the topical application of zinc oxide was found to promote the healing processes of chronic and surgical wounds.[8] Furthermore, its ability to filter UV light is widely exploited in the use of sun screens and cosmetics.[9] On the other hand, excess zinc can have a number of undesirable effects. It is one of the culprits in inducing metal fume fever, an illness caused by the inhalation of metal fumes in foundry workers.[10] It is also becoming increasingly clear that Zn^{2+}, like Ca^{2+}, is an essential signaling molecule for a number of physiological processes, with cellular zinc homeostasis being tightly controlled. Alterations in brain zinc levels are now thought to contribute to neurodegeneration in conditions, such as Alzheimer's disease, amyotrophic lateral sclerosis, and ischemia.[11−13] Recently, the use of zinc and titanium oxide nanomaterials in cosmetics and sunscreens has also been called into question.[14]

ZnO nanoparticles (NPs) have been shown previously to cause toxicity, and in many cases, this has been related to the release of ionic zinc.[15−20] However, these studies have mostly studied spherical ZnO NPs, and it has been shown that 1D structures, such as nanowires, exhibit very different dissolution behavior. ZnO is very sensitive to dissolution in acidic conditions, and the phase diagram indicates that it should dissolve below a pH of 6.7 at physiological temperature.[21] However, ZnO nanowires tend to have a high aspect ratio along their polar (0001) direction, and this surface is much more unstable than the other faces of the crystal. The result of this is that the dissolution of ZnO nanowires is extremely anisotropic, with the material dissolving primarily down its polar surface.[22] Charged adsorbents in the cell may block or enhance this behavior as has been shown by the co-investigators for specific anions,[23] which may affect their biostability and ultimately toxicity. So far, the behavior of high aspect ratio ZnO nanowires in biological systems and the effects of various physiological factors on the rate and mode of dissolution have hardly been studied.

In this paper we will discuss the toxic effects of ZnO nanowires on human macrophage cells in the context of a pH-triggered release of metal ions within the cell. The uptake and morphological evolution of the ZnO is assessed using a range of microscopic techniques, and a complementary *in vitro* study of the dissolution kinetics in simulated biofluids (SBFs) of lysosomal and extracellular pH will be presented. Morphology evolution in SBFs will be compared to intracellular dissolution assessed by transmission electron microscopy (TEM), scanning electron microscopy (SEM), and confocal microscopy of live cells using the zinc ion-specific fluorescent dye FluoZin3-AM. Human monocyte-derived macrophages were chosen as an *in vitro* model for the exposure of nanowires to cells, as these cells form the first line of defense in the immune response to foreign materials in many tissues, including the lung, and have large pro-inflammatory potential. Macrophages are differentiated in culture and fairly long-lived, do not proliferate, and are highly phagocytic, often ingesting vast amounts of foreign material. This also makes them ideal candidates for biodegradation studies looking at the long-term fate of ingested particles inside cells.

RESULTS AND DISCUSSION

Particle Characterization. High aspect ratio ZnO nanowires were synthesized by electrodeposition into polycarbonate templates with defined pore sizes, sputter-coated on one side with a thin layer of gold. This produced ZnO nanowires of uniform size as shown by SEM before removal from the gold layer (Figure 1A). The wires had a slightly tapering shape with a broad tip and a narrower base. Purification and separation of the wires from their templates using dichloromethane (DCM) caused some breakages, creating preparations with a wider variation in length. Particle dimensions were established using TEM, and the results for the various ZnO batches are summarized in Table 1. Thickness for most nanowires was typically around 120 nm, with the length ranging from ~2 μm for some templates to ~5 μm for others, depending on the duration of the electrodeposition process. In the case of ZnO/3, the deposition time was extended, creating wires of ~10 μm in length and ~330 nm in thickness (Figure 1B). The length of ZnO nanowires given in the Table 1 refers to the maximum length, before the induction of breakages. Figure 1B also shows the tendency of the ZnO nanowires to form aggregates, which are hard to disperse. Figure 1C shows the microstructure of pristine ZnO nanowires revealing a smooth and crystalline surface. High-resolution TEM (HR-TEM) revealed a regular lattice structure demonstrating that some areas of the wires are monocrystalline in nature (Figure 1D), whereas many areas appear polycrystalline (Figure 1E, arrowheads). The lattice spacings of ~5.2 and 2.9 Å (Figure 1D) are consistent with ZnO nanowires exhibiting a Wurtzite structure in agreement with the Fourier transform (FT) pattern obtained from the sample in Figure 1F. Phase identification and purity were confirmed by synchrotron-based X-ray diffraction (not shown). In all cases only the Wurtzite lattice (predominantly with (0002) texture, Figure 1F) and the Au substrate (with (111) texture) peaks were observed. These ZnO batches, liberated from their synthesis template, were used for the cell culture experiments

Cytotoxicity of ZnO Nanowires to Human Monocyte Macrophages (HMMs). The toxicity of ZnO nanopowders to mammalian cells in culture has been investigated in several studies. Globular or lozenge-shaped ZnO NPs in the 10−200 nm size range were toxic to mouse neuronal stem cells after 24 h at concentrations above 12

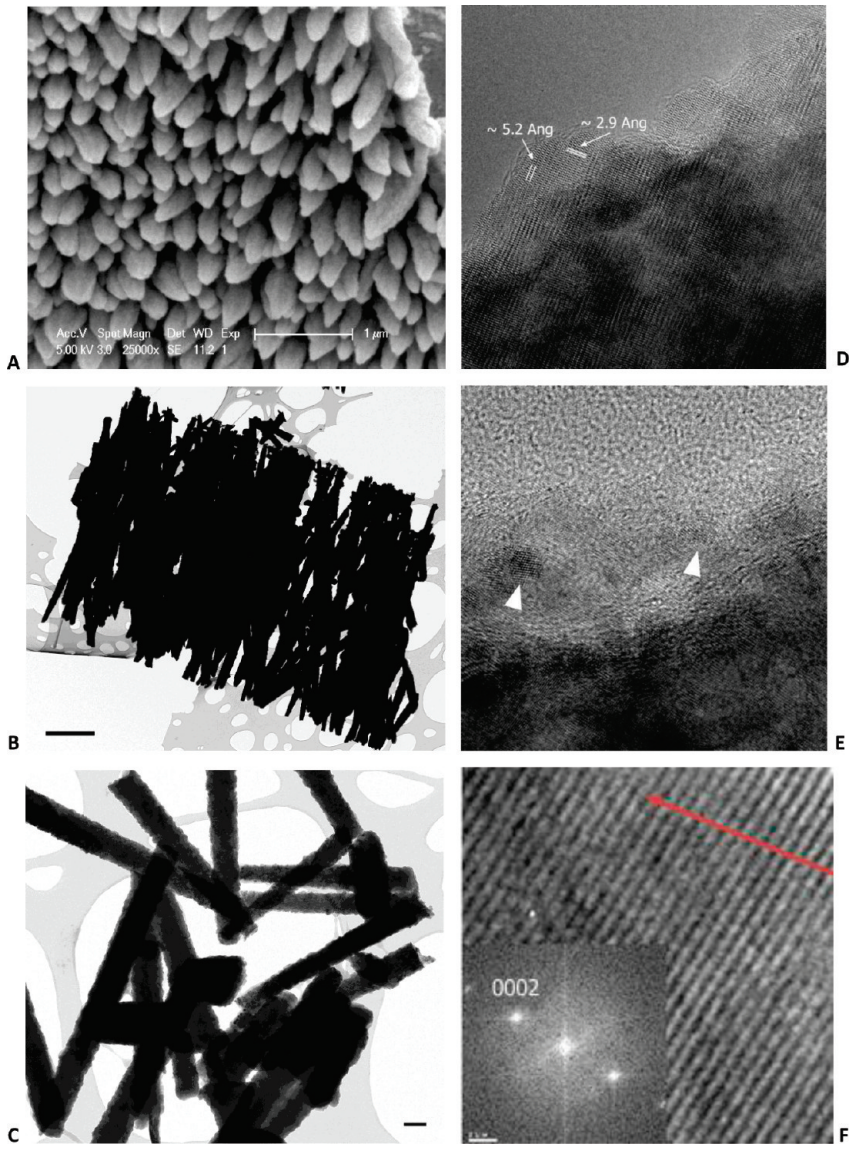

Figure 1. Characterization of ZnO nanowires. (A) SEM of ZnO nanowires on the gold layer after removal of the polycarbonate template with DCM. (B) TEM of purified ZnO nanowires showing aggregation (scale bar = 2 μm). (C) TEM of purified ZnO nanowires showing a smooth surface (scale bar = 100 nm). (D and E) HR-TEM images revealing ZnO nanowire lattice structure and mono- and polycrystalline areas. (F) High-magnification lattice image and corresponding FT showing the textured nature of the nanowire with (0002) growth direction being the most dominant. The red arrow indicates the long axis of the nanowire.

ppm. Toxicity was independent of particle size and similar to $ZnCl_2$, indicating that ionic zinc may be responsible.[20] Nano-ZnO was also found to be toxic to rat macrophages, human bronchial epithelial cells,[18] and primary mouse embryonal fibroblasts.[19] Rod-shaped ZnO nanoparticles with lengths of 100−200 nm and diameters of 20−70 nm were toxic to human aortic endothelial cells at 10 and 50 μg/mL.[24] In the human lung epithelial cell line A549, ZnO particles of 70 and 420 nm were toxic after 24 h with EC_{50} values of 13.6 and 14.2 μg/mL, respectively.[25]

TABLE 1. Particle Dimensions of ZnO Nanowire Batches

nanowire batch	ZnO/3	ZnO/4	ZnO/5	ZnO/6	ZnO/7
thickness (nm, ± SE)	327 ± 3	123 ± 1	118 ± 1	121 ± 1	111 ± 1
number counted	n = 1004	n = 763	n = 517	n = 557	n = 677
length (μm)	~10.5	~5.2	~2.1	~4.0	~4.5

In our study in HMMs, the cytotoxicity of high aspect ratio ZnO nanowires (ZnO/3) and $ZnCl_2$ was assessed using the neutral red assay, which measures the accumulation of neutral red dye in the lysosomes of live cells. Zinc in $ZnCl_2$ solutions was considered to be in the form of soluble, ionic Zn^{2+}, whereas zinc from ZnO nanowires was deemed to be predominantly in the form of insoluble zinc oxide. When compared to the no additions (NA) control, $ZnCl_2$ was significantly toxic to HMMs after 24 h at concentrations of 10, 20, and 40 μg/mL (Figure 2A). Cell viability with ZnO was reduced to similar levels, although only the concentration of 20

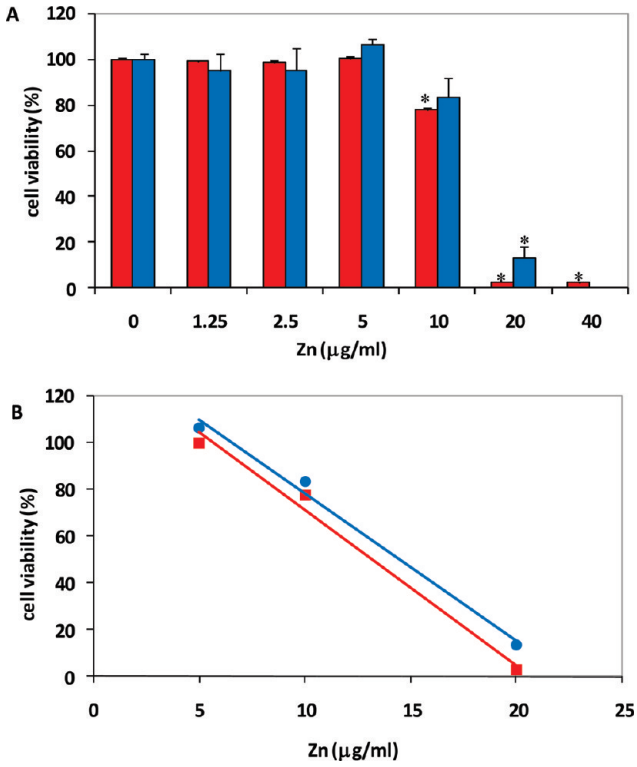

Figure 2. ZnO nanowire toxicity. HMMs were incubated with medium only or with the indicated concentrations of zinc in the form of $ZnCl_2$ or ZnO/3 (red or blue bars, respectively) for 24 h. Subsequently, cell viability was assessed using the neutral red assay (A). Results represent the mean ± SE of four ($ZnCl_2$) or two (ZnO/3) experiments, respectively. Each experiment was performed in triplicate. Asterisk (*) denotes $p \leq 0.01$ compared to that of the NA controls. (B) Scatter plot with linear trend lines for $ZnCl_2$ and ZnO/3 (red and blue lines, respectively) in the concentration range of 5−20 μg/mL.

μg/mL was statistically significant. Due to the scarcity of the nanowire material, the highest concentration of 40 μg/mL was not tested. When compared to each other, there was no statistically significant difference between $ZnCl_2$ and ZnO toxicity at any of the concentrations tested. The scatter plot in Figure 2B shows the linear trends for $ZnCl_2$ and ZnO ($R^2 = 0.9873$ and 0.9908, respectively) toxicity at concentrations of 5, 10, and 20 μg/mL. The resulting LC_{50} values were 13.2 and 14.5 μg/mL for $ZnCl_2$ and ZnO, respectively, which is similar to the studies on ZnO nanopowders mentioned above. This suggests that toxicity of ZnO nanowires is due to the release of ionic zinc rather than to the high aspect ratio of the wires.

Only a few other studies have investigated the toxicity of ZnO nanowires. Cell adhesion and spreading of NIH3T3 fibroblasts, human umbilical vein endothelial cells, and bovine capillary endothelial cells were reduced on ZnO nanorod surfaces of ~50 and ~500 nm thickness and length, respectively, with a concomitant decrease in cell viability.[26] In a similar study, mouse macrophages initially settled and spread on the ZnO nanorod surfaces. However, a significant degree of necrosis was apparent after ~6.5 h of incubation. Inductively coupled plasma mass spectrometry (ICP-MS) of cell culture media showed Zn^{2+} release from the ZnO surfaces, indicating that toxicity was caused by ionic Zn^{2+} rather than nanowire topography.[27] Monitoring NP toxicity using dye-based toxicity assays alone can be problematic due to dye−NP interactions, which can lead to false-positive results.[28] The interaction of ZnO nanowires with the neutral red dye was not assessed in our study due to their scarcity. Instead, cytotoxicity was confirmed using additional techniques, such as confocal fluorescence microscopy and bright-field TEM (BF-TEM) (see below).

Confocal Live Imaging—Rise of Intracellular Zn^{2+} Precedes Cell Death. Uptake and cytotoxicity of ZnO nanowires (ZnO/4) was further investigated using confocal laser microscopy of live cells. HMMs were preloaded with the Zn^{2+} indicator FluoZin3-AM. This cell-permeant AM ester (acetoxymethyl) is cleaved by intracellular esterases, becomes cell-impermeant, and displays green fluorescence upon binding of ionic Zn^{2+}. Binding of FluoZin3 to solid ZnO nanowires is unlikely as fluorescent ZnO nanowire aggregates were never observed during our confocal experiments. Subsequent to dye loading, cells were incubated with sample solutions, and images were acquired over a time period of ~5−6 h. The red fluorescent dye propidium iodide (PI), which is excluded by live cells, was added to stain the nuclei of dead cells. For analysis, fluorescence intensities were measured and averaged within 10 regions of interest (ROIs) for each sample to create a general overview of the culture (not shown). Using these data, a representative ROI was chosen for each sample, and single cell traces are shown in Figure 3. The insets are movie stills taken at the 5 h time points and give an overview of the cultures. In the NA-control (Figure 3A), cells were incubated with imaging buffer only. No increase in FluoZin3- or PI-fluorescence was observed over time (see inset Figure 3A after 5 h), indicating that the cells did not suffer fatal laser irradiation damage or that the Zn^{2+} indicator started to fluoresce over time in the absence of zinc (47 cells/frame, 0 cells PI positive, and 0% cell death). Incubation with 20 μg/mL $ZnCl_2$ (Figure 3B) resulted in an increase of FluoZin3 fluorescence in a diffuse pattern in the cytoplasm, indicating a rise in intracellular Zn^{2+} concentrations. Most cells in the field of view reacted fairly synchronously (see inset Figure 3B after 5 h). After ~4−5 h, numerous cells started to show extensive plasma membrane swelling, followed by a sharp drop in FluoZin3 fluorescence, probably indicating the leakage of the Zn^{2+}−dye complex from the cells. Concomitantly, an increase in PI fluorescence was observed indicating cytotoxicity (47 cells/frame, 7 cells PI positive, and 14.9% cell death after 340 min). In contrast, incubation of HMMs with 20 μg/mL ZnO (Figure 3C) showed a much more heterogeneous reaction (see inset Figure 3C after 5 h); some cells died as early as 2 h postexposure, and some died around the 5 h time mark. This may be explained by the particulate nature of the

ZnO nanowires and by their tendency to aggregate, which can expose cells locally to variable concentrations of ZnO. Cytotoxicity was characterized by a steep increase in FluoZin3 fluorescence inside the cells, probably due to the rapid intracellular dissolution of the ZnO. This was followed by cell swelling and a drop in FluoZin3 fluorescence accompanied by the increase in PI fluorescence (36 cells/frame, 5 cells PI positive, and 13.9% cell death after 340 min). The live imaging results for controls, $ZnCl_2$ and ZnO, incubations are best viewed in movie form (Supporting Information, Figure S1). These results suggest that the cytotoxicity of ZnO is due to increases in ionic Zn^{2+} following entry of the nanowires into the cell. Cell morphology suggested necrosis as the path of cell death, similar to the study of Zaveri *et al.*[27] The occurrence of early deaths indicates that nanowire dissolution may start quite rapidly.

ZnO Nanowire Dissolution in Simulated Body Fluids. Several studies[15−17,19,20] have shown that the toxicity of globular ZnO NPs is due to the release of ionic zinc. However, in most cases it was unclear whether dissolution occurs in the extracellular medium before uptake or intracellularly following ingestion. Xia *et al*. suggest that ZnO NP dissolution can occur in the extracellular medium as well as intracellularly.[18] In order to address this issue in our study, ZnO nanowires were exposed to two different simulated body fluids (SBFs) *in vitro*: SBF similar in ionic composition and pH to extracellular fluid (ex-SBF, pH 7.4) or SBF more akin to lysosomal fluid (lyso-SBF, pH 5.2). Neither SBF contained any protein. After incubation of ZnO nanowires in SBFs for 30 min at 37 °C, solutions were filtered to remove nondissolved ZnO nanowires. The amounts of total Zn and dissolved ionic Zn^{2+} were quantified by ICP-MS (Figure 4, top panel). In ex-SBF pH 7.4, only 4.45% (SE ± 0.006) of Zn was found in the dissolved fraction, whereas in lyso-SBF pH 5.2 the ionic Zn^{2+} fraction constituted 99.33% (SE ± 0.19) of the total. The Zn concentrations of SBFs and DCM solvent controls were near the detection limit (not shown). The ratio of ZnO: solvent (respective SBF) for the dissolution experiments was approximately 1:3819 (w/w), indicating that the buffers were in vast excess. The ready solubility of ZnO under acidic conditions is well-known, and the thermodynamic behavior of zinc in aqueous solution has been described in detail.[29] Our results using SBFs for dissolution show that ZnO nanowires, if taken up by cells, could dissolve rapidly at lysosomal pH, whereas dissolution in the extracellular medium would be comparatively slow.

We also studied the dissolution of ZnO nanowires in SBFs by TEM. After 30 min in ex-SBF pH 7.4, no significant changes to the morphology of ZnO nanowires were apparent indicating that there was little dissolution (Figure 4A). In contrast, after only 10 s in lyso-SBF pH 5.2, the nanowires showed a jagged and irregular surface and started to break up. After 2 min, virtually no nanowires were left on the grid (not shown). Zhou *et al*. have studied the dissolution of ZnO in a range of solutions by SEM.[1] The etching process usually started at the edges of the hexagonal wires, leaving the flat surfaces initially spared, resulting in a jagged appearance of the wires similar to the morphology seen in our study in SBFs. In the presence of serum, the dissolution rate was decreased, and the nanowire surface appeared smooth during dissolution,[1] indicating that protein interaction can affect this process. The inhomogeneous nature of the dissolution is related to the effect of local environmental species on the ZnO wurtzite lattice; this

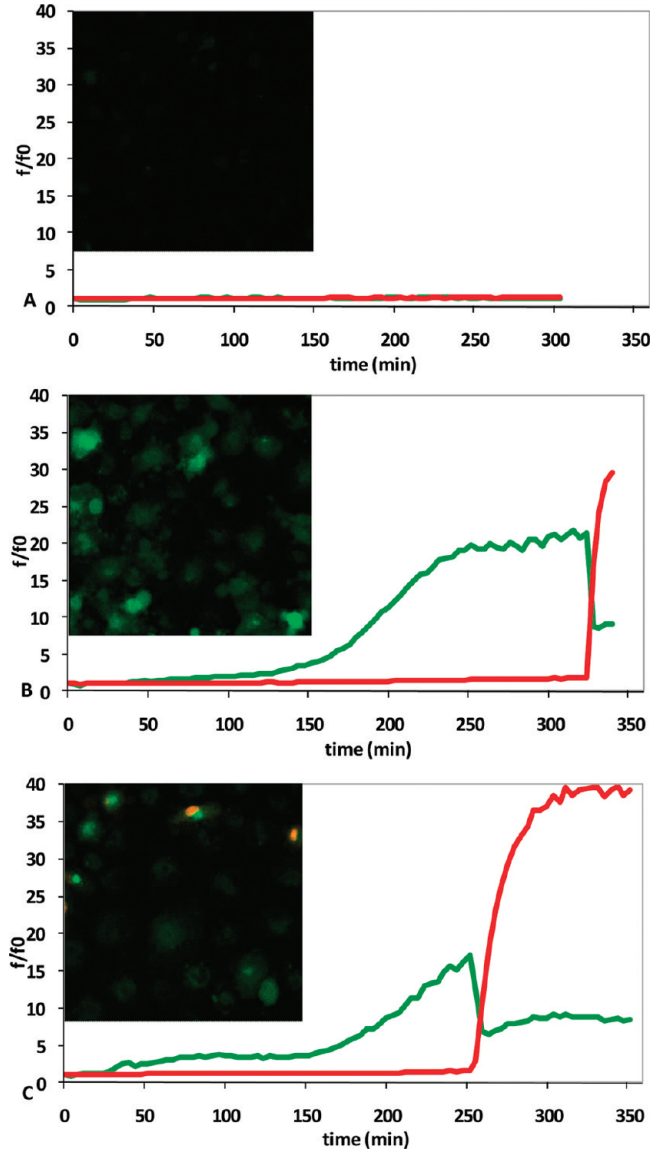

Figure 3. Confocal live imaging. HMMs were loaded with the cell-permeant Zn^{2+} indicator FluoZin3-AM (green fluorescence) prior to incubation with (A) imaging buffer (NA control), (B) 20 μg/mL $ZnCl_2$, or (C) 20 μg/mL ZnO/4. PI was included to stain the nuclei of dead cells. Images were acquired over a time course of ~5−6 h. Fluorescence intensities were measured within a representative region of interest and expressed as *f*/*f*0 (*f*0 = fluorescence intensity in arbitrary units at *t* = 0). Insets are movie stills after 5 h of incubation and illustrate the homo/heterogeneity of the cellular responses to $ZnCl_2$ and ZnO nanowires, respectively. Movies are shown in Figure S1 in the Supporting Information

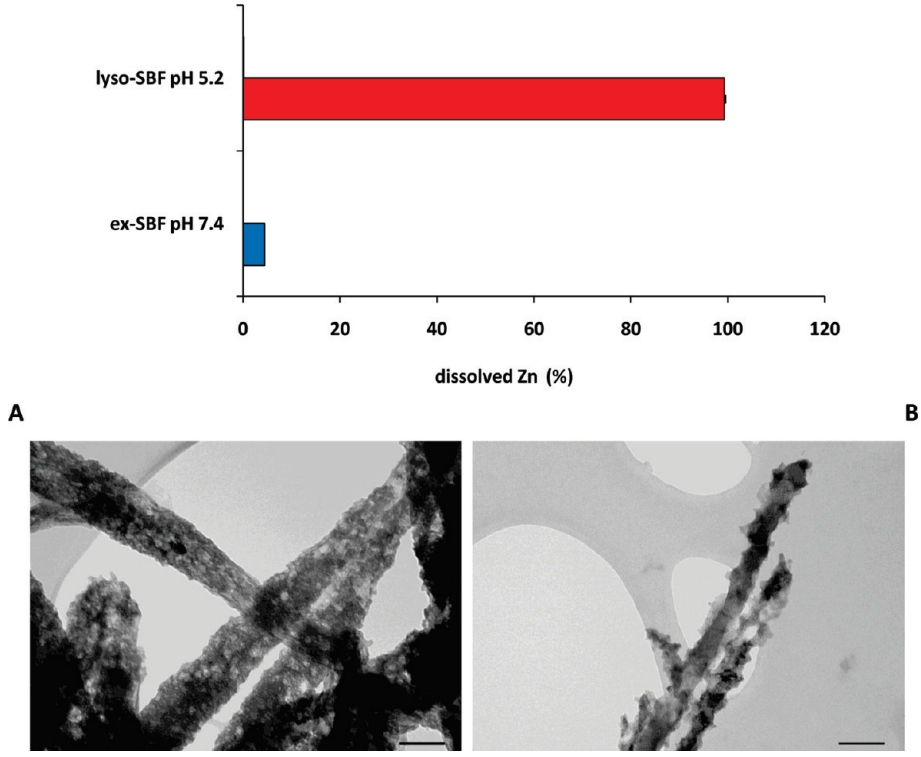

Figure 4. Dissolution of ZnO nanowires (ZnO/6) in SBFs. Top graph: purified ZnO nanowires were incubated in ex-SBF pH 7.4 or in lyso-SBF pH 5.2 for 30 min prior to analysis of total and dissolved zinc by ICP-MS. Values represent the percentage of dissolved zinc (mean ± SE of triplicate measurements). Bottom panel: purified ZnO nanowires were incubated in ex-SBF pH 7.4 for 30 min (A) or in lyso-SBF pH 5.2 for 10 s (B) before imaging by TEM. Scale bars are 100 nm.

has both polar and nonpolar faces which exhibit different rates of dissolution and which can be differentially stabilized by specific adsorption.[23]

Uptake and Dissolution of ZnO Nanowires in HMMs. Many studies investigating the toxicity of small size, globular ZnO NPs lack TEM imaging data. This may be due to the fact that the smaller particles either dissolve more rapidly or cannot be identified inside the cells due to their small size. In human bronchial epithelial cells, fluorescently labeled ZnO NPs were located to caveoli, whereas in RAW264.7 macrophage cells, they were found in lysosomes.[18] In human aortic endothelial cells, ZnO NPs were mostly bound at the cell surface,[23] whereas they were located in endosomes in human lung epithelial cells.[25]

In our study, HMMs were incubated with 50 μg/mL ZnO nanowires (ZnO/3) for 1 h to allow uptake to take place. Then, cells were washed and either fixed immediately (0 h time point) or cultured on in the absence of nanowires for various lengths of time before processing for TEM (Figure 5). At the earliest time point (Figure 5A and B), the wires often appeared almost transparent, probably due to dissolution of the extremely acid-labile ZnO during TEM sample processing, complicating the interpretation of intracellular dissolution. Nevertheless, it was clear that cells avidly phagocytised large aggregates of the nanowires within 1 h of exposure (Figure 5A). A thin, electron-dense layer was visible on their surface (Figure 5B, arrows) indicating material/protein deposition. This material could be derived from the cell culture medium, the cells, or both. Extremely electron-dense material was present at the pointed end of the nanowires, probably some gold remnants from the synthesis template (Figure 5B, arrowheads). After 1 h of chase, numerous cells contained intracellular bundles of nanowires, which were contained within membrane-bound organelles, probably phagosomes or lysosomes. In some cells, electron-dense staining appeared at the margins of the wires, which had the appearance of crystalline precipitates (Figure 5C and D). The formation of these crystalline deposits could be due to supersaturation of the lysosomal contents with zinc during dissolution of the comparatively large nanowires in the small volume of the lysosomes. After 4 h, the intracellular nanowires were often surrounded by round structures, which could represent small vesicles or protein precipitates (Figure 5F, arrows). After 24 h of chase, cells frequently contained numerous aggregates of ZnO nanowires, the outline of which was still preserved and smooth in appearance (Figure 5G and H), although it was not clear whether zinc was left in these 'ghost' structures. Nanowire structures were still contained within membrane-bound compartments (Figure 5H, arrows), and in some places, the round, vesicular structures were still found in their vicinity (Figure 5H, arrowheads). Increasingly, the wires were uniformly electron dense through their entire thickness showing that deposition and pervasion of

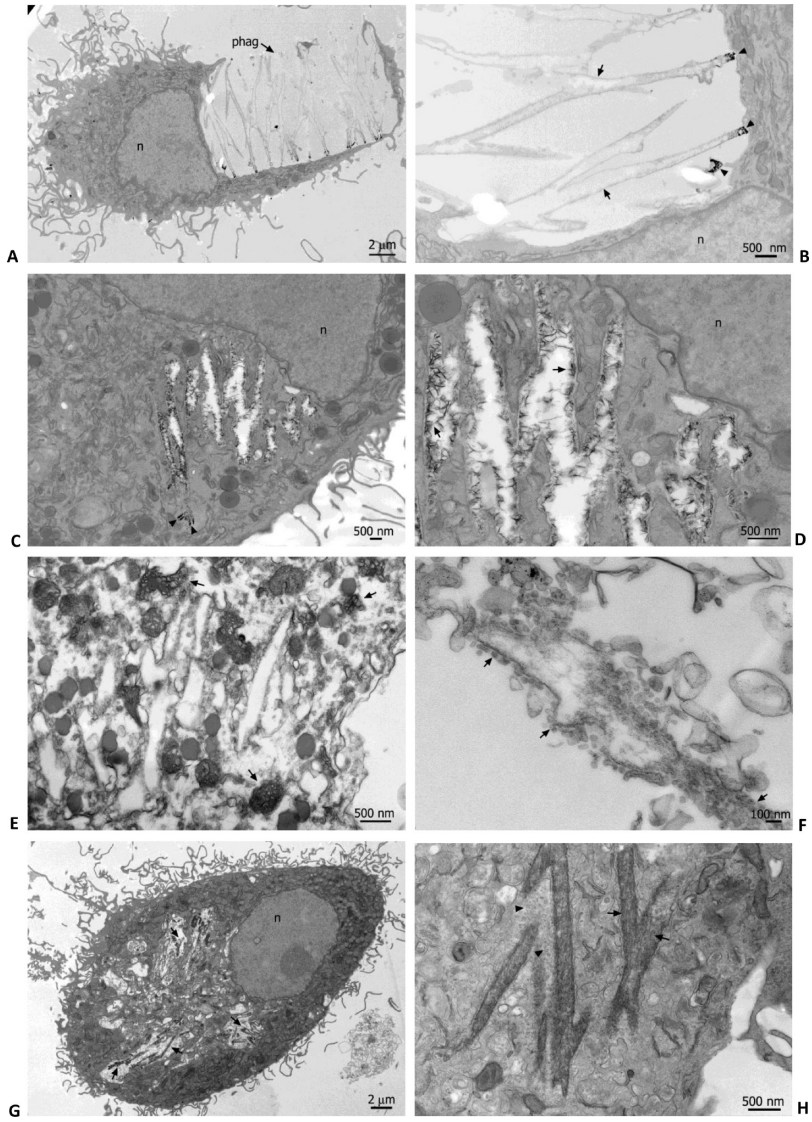

Figure 5. BF-TEM of HMMs after exposure to ZnO. Cells were incubated with ZnO for 1 h, washed, and either fixed immediately (A and B) or cultured on in the absence of nanowires for 1 h (C and D), 4 h (E and F), or 24 h (G and H) prior to processing for TEM (n = nucleus).

ZnO nanowires with electron dense, organic material had taken place during the 24 h. Energy-filtered TEM (EF-TEM) jump ratio mapping at the Zn L2,3 edge indicated that the crystalline precipitates observed in Figure 5C and D remained Zn-rich (see Figure 6).

The preservation of ZnO nanowire 'ghosts' seen in our study in HMMs could be explained in two ways: First, interaction of cellular components with the wires may affect their dissolution rate and morphology in a similar manner as observed *in vitro* in the presence of serum.[1] Upon incubation with plasma, ZnO NPs were shown to bind a range of plasma proteins *in vitro*.[30] Anisotropic dissolution, characterized by a hollowing out of the ZnO nanowires to form hexagonal tubes, has been reported to occur *in vitro*.[22,23] It is not certain from TEM imaging whether this mechanism is responsible for ZnO nanowire dissolution in our study due to technical limitations. Imaging by 3D electron tomography may be able to answer this question. Alternatively, the preservation of ZnO nanowire 'ghosts' may be due to a fixative effect of ionic Zn^{2+} upon release from the nanowires. The rounded, electron-dense structures near the nanowires visible in TEM may represent such protein precipitates. Zinc-based fixatives are finding increasing application for tissue fixation in histopathology, although the exact molecular basis of the fixation process is still unknown.[31]

ZnO Nanowire Dissolution in HMMs. It seemed clear from TEM imaging that some ZnO dissolution had taken place during TEM sample processing. We therefore also used SEM and energy-dispersive X-ray spectrometry (EDX) analysis (Figure 7) to study ZnO nanowire uptake and dissolution in HMMs (ZnO/4). Cells were incubated with 50 μg/mL ZnO for 1 h and were either processed immediately (0 h time point, Figure 7B) or cultured on in the absence of nanowires for 4 or 24 h

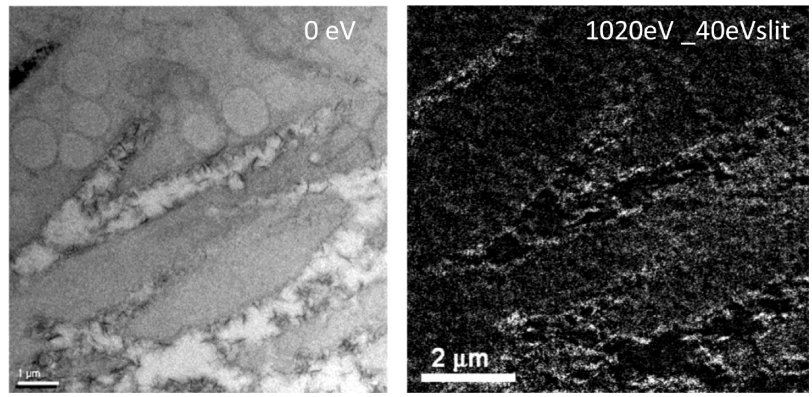

Figure 6. Analysis of electron-dense deposits by EF-TEM. After a pulse (1 h) with ZnO nanowires, HMMs were cultured in the absence of nanowires for 1 h before processing for TEM. Electron-dense, crystalline deposits were found inside the cells by BF-TEM (left). Analysis by EF-TEM showed that these deposits (light-colored areas in image on the right) are still Zn-rich (Zn L2,3 edge jump ratio maps using a 40 eV energy slit and using pre- and postedge energy windows centered at 995 ± 20 and 1040 ± 20 eV, respectively).

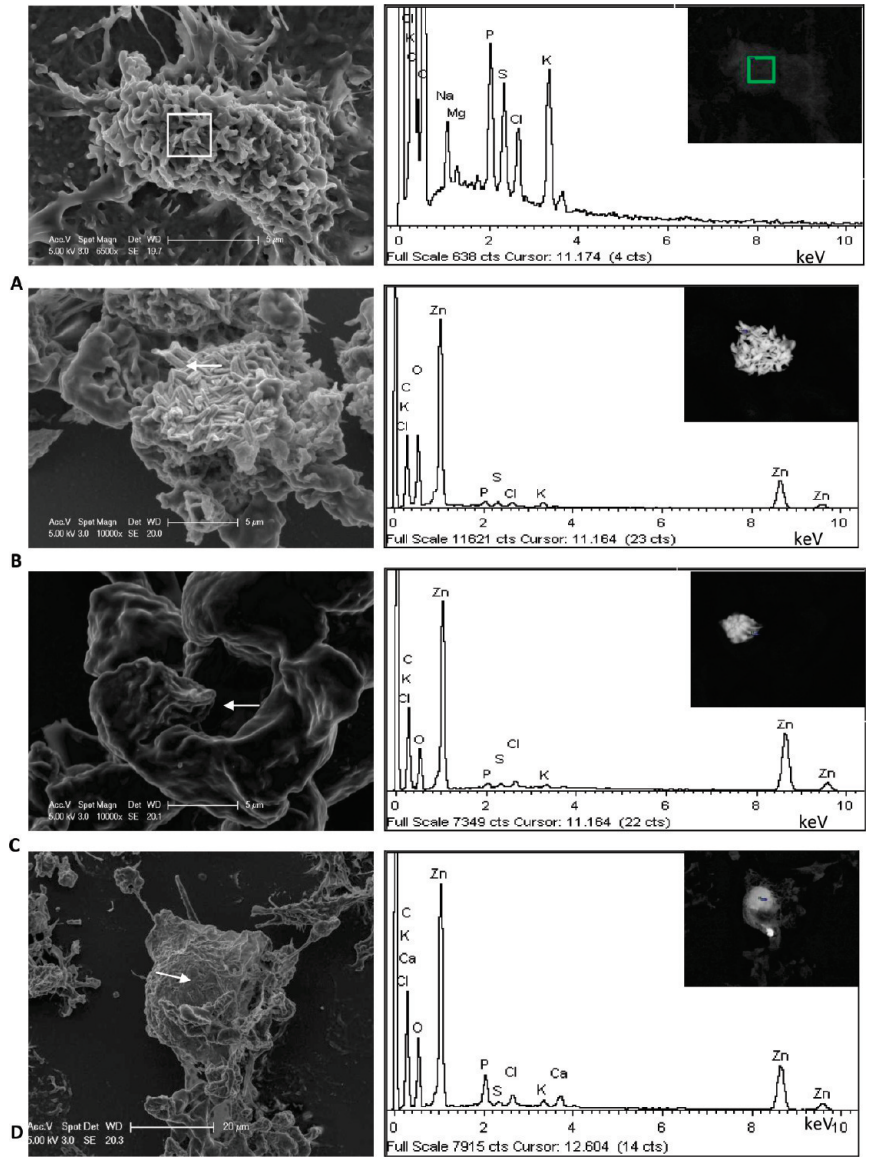

Figure 7. SEM and EDX analysis of ZnO uptake in HMMs. Cells were incubated with culture medium only (A) or with ZnO nanowires for 1 h. Then, cells were either processed immediately (B) or cultured on in the absence of ZnO for 4 h (C) or 24 h (D). Images on the left (SE detector) show cells in detail; panels on the right are corresponding EDX spectra with their respective high *Z*/BSE images.

(4 and 24 h time points; Figure 7C and D, respectively). However, after the exposures, cells were immediately quench-frozen and freeze-dried, which should minimize any dissolution artifacts to the ZnO nanowires during processing. Samples were first screened using the backscatter electron (BSE) detector at 20 keV to locate areas with high atomic number (*Z*), and spectra were acquired in those areas (Figure 7, spectra and insets). Subsequently, high-resolution images of these areas were taken at 5 keV using the secondary electron (SE) detector (Figure 7, images on left).

No areas with high *Z* were located in the NA controls (Figure 7A), and no zinc peaks were present. In contrast, many areas with high *Z* were found in the 0 h time point. In Figure 7B, a larger aggregate of ZnO nanowires can be seen on the surface of the cell, probably in the process of phagocytosis. The corresponding EDX spectrum clearly shows the presence of zinc. After a 4 h chase period, areas with high *Z* were harder to find, indicating that ZnO dissolution was taking place. In Figure 7C, an intracellular ZnO aggregate is pinpointed by the arrow; the corresponding EDX spectrum confirms the presence of zinc. After a 24 h chase period, only a single intracellular area with high *Z* could be found in the sample (Figure 7D), which was confirmed as zinc, whereas the vast majority of cells lacked a zinc peak. This indicates that after 24 h, most ZnO nanowires had been dissolved by the cells. Occasionally, areas of high *Z* showed the presence of gold, representing remnants of the synthesis template (not shown). After the 24 h chase period, no zinc peaks were detected in intracellular areas of low *Z*. This could indicate that ionic zinc is exported from the cells or that it leaches out due to membrane damage. Alternatively, intracellular, dispersed Zn^{2+} concentrations may be too low to produce a signal in SEM/EDX.

Mode of Cell Death Induced by ZnO Nanowires. In the neutral red assay, incubation of HMMs with ZnO nanowires and $ZnCl_2$ resulted in very similar toxicity profiles. This may seem surprising, considering that zinc delivery to the cells probably differs between the two compounds. Soluble, ionic Zn^{2+} from $ZnCl_2$ may simply enter the cells by diffusion across the plasma membrane or through ion channels in a homogeneous manner throughout the culture. In contrast, uptake of ZnO nanowire aggregates by phagocytosis results in a fairly heterogeneous delivery of zinc to HMMs, with some cells receiving vast amounts and others maybe very little. In our opinion, the similarity of toxicity profiles in the neutral red assay after 24 h is caused by the rapid uptake of ZnO nanowires by HMMs (as seen in TEM), rapid intracellular dissolution at acidic pH (Figures 3 and 4), and spillage of free, ionic Zn^{2+} into the surrounding culture medium. Zn^{2+} released from dying cells is then free to exert more cytotoxicity to neighboring cells in the culture. SEM/EDX confirmed that hardly any intact ZnO nanowires were present in cells at this time point. However, the neutral red assay allows no distinction between different modes of cell death, *i.e.*, necrosis versus apoptosis, and therefore this was assessed using imaging techniques.

Cytotoxicity observed by live imaging confocal microscopy in HMMs showed features of necrosis, such as cell swelling. Cell ultrastructure after incubation with ZnO nanowires was monitored in more detail by BF-TEM. Exposure of HMMs to ZnO nanowires led to severe structural changes in the cells (Figure 5A−H). At the 0 and 1 h time points (Figure 5A−D), the cells generally still appeared healthy with numerous cell surface protrusions and a finely granular nucleus. The cytoplasm contained extensive endoplasmatic reticulum and normal mitochondria with a slightly electron-dense matrix and an extensive cristae. After a 4 h chase period, some of the cells showed signs of toxicity (Figure 5E) with some characteristics of necrosis, such as a leached-out cytoplasm. In contrast, mitochondria typically showed a very electron-dense matrix and swelling (Figure 5E, arrows), changes more reminiscent of apoptosis. After 24 h of chase, the overall culture was quite heterogeneous, with some cells showing severe toxicity, while others still had a fairly healthy morphology; quite similar to the results seen in the live imaging experiments. For comparison, the effect of ionic Zn^{2+} on the ultrastructure of HMMs was also tested (Figure 8). Control cells showed a normal morphology with healthy mitochondria, as described above (Figure 8A and B arrows). With increasing concentrations of $ZnCl_2$, HMMs displayed morphological changes indicative of cytotoxicity with increasing severity. After exposure to $ZnCl_2$ solutions of 6 μg/mL Zn concentration, cells started to lose surface protrusions, and the nuclear chromatin became more condensed. The matrix of mitochondria became more electron dense, and their cristae started to swell (Figure 8C, D arrows). After 24 h with 8 μg/mL Zn, the cells started to show cell surface blebbing, a highly lobular nucleus with increasing chromatin condensation and highly pyknotic mitochondria (Figure 8E and F arrows), indicative of apoptosis. At the top concentration of 12 μg/mL Zn, the cells were largely necrotic with leached out cell contents and highly condensed nuclear chromatin. Individual cytoplasmic organelles, including mitochondria, were almost unrecognizable (Figure 8G and H arrow). Taken together, HMMs treated with either ZnO wires or $ZnCl_2$ show signs of apoptosis, such as chromatin condensation and mitochondrial pyknosis as well as signs of necrosis, such as plasma membrane rupture and leaching of cytoplasmic contents. In the case of $ZnCl_2$, apoptosis was more often seen at lower zinc concentrations, whereas necrosis was a more prominent feature at higher concentrations. In the case of ZnO wires, the cells will have been exposed locally to highly variable concentrations of zinc, explaining the presence of necrotic as well as apoptotic features in our study. There-

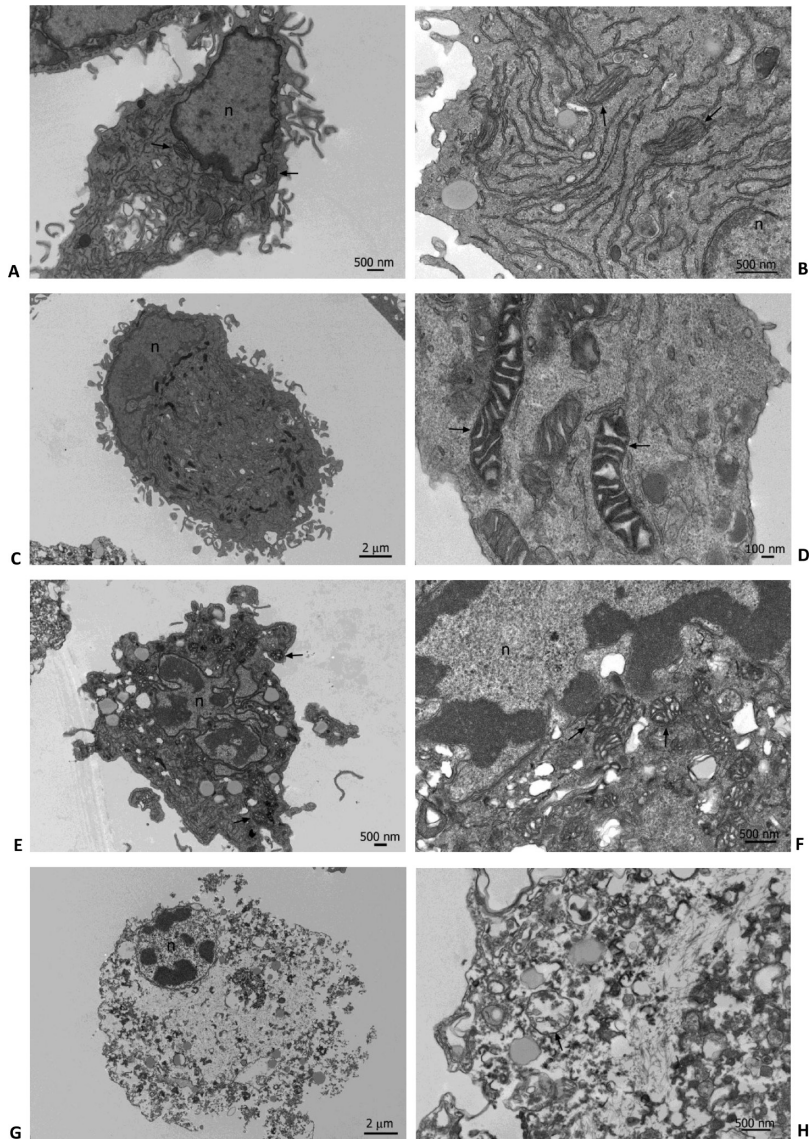

Figure 8. BF-TEM of HMMs after $ZnCl_2$ exposure. HMMs were incubated with medium only (A and B) or with 6 μg/mL (C and D), 8 μg/mL (E and F), or 12 μg/mL (G and H) $ZnCl_2$ for 24 h. Arrows point to mitochondria (n = nucleus).

fore, although soluble, ionic Zn^{2+} is the toxic species in both cases, the mode of cell death and with it cellular ultrastructure can vary depending on the speed and severity of the toxic insult.

Zinc's role in apoptosis is complex, and it has been found to inhibit as well as induce it.[32] Apoptosis was observed in a variety of neuronal cell types due to zinc dyshomeostasis.[11−13,20,33] One possible target for zinc action is inhibition of cellular energy production with effects on the electron-transport chain, the mitochondrial membrane potential, and the induction of mitochondria permeability transition.[34,35] This may explain the ultrastructural changes to HMM mitochondria observed in our TEM studies. In addition, ZnO NPs have been shown to induce cell death by inducing ROS production, lipid peroxidation, and DNA damage.[18,19,36] Considering the number of cellular processes and signaling pathways zinc is involved in, it is not surprising that zinc dyshomeostasis can induce cell death by different pathways depending on concentration, conditions, and cellular target.

Implications for ZnO Nanowire Applications. The combination of intracellular dissolution and resulting cytotoxicity from ionic Zn^{2+} observed in this study could make ZnO nanowires potential candidates for drug targeting, if dissolution rate and delivery could be modulated and controlled. Doping of ZnO nanowires with other elements, such as cobalt or manganese, may affect their dissolution rates and degree of toxicity. George *et al.* have shown that doping of ZnO nanoparticles with iron slows down their dissolution rate and concomitantly their cytotoxicity to endothelial and macrophage cells in culture.[37] Protein adsorption onto ZnO NPs has been shown to depend on the surface charge of the particle and the protein. Incubation in cell culture medium resulted in protein and Ca^{2+} adsorption onto the ZnO

NPs, which affected their cytotoxicity.[38] In the cyanobacterium *Anabaena flos-aquae* and the protist *Euglena gracilis*, coating of ZnO NPs with different protective layers led to changes in uptake pattern and to variable effects on photosynthetic activity and viability.[39] Phosphonic acids were used to link specific targeting antibodies to ZnO nanowires, which indicates that functionalization of ZnO nanowires is feasible.[40] Leakage of Zn^{2+} into the systemic circulation due to dissolution of ZnO vectors would probably be well tolerated as reports of zinc toxicity to humans are rare. In fact, 8−11 mg/day is the recommended daily allowance for zinc in adults in the United States.[41]

CONCLUSIONS

Our study shows that high aspect ratio ZnO nanowires are cytotoxic to human monocyte macrophages (HMMs) in culture at similar concentrations as $ZnCl_2$, indicating that ionic Zn^{2+} is released resulting in the observed toxicity. Confocal fluorescence microscopy confirmed a rise in intracellular, free Zn^{2+} prior to cell death. Inductively coupled plasma mass spectrometry (ICP-MS) analysis measured rapid dissolution of ZnO nanowires in simulated biofluids (SBFs) of lysosomal pH, whereas comparatively little dissolution was occurring at extracellular pH, demonstrating that ZnO nanowire dissolution occurs primarily inside the cells. Bright-field transmission electron microscopy (BF-TEM) showed rapid uptake of ZnO nanowire aggregates in HMMs by phagocytosis and intracellular dissolution within a membrane-bound compartment, probably lysosomes. Dissolution of ZnO nanowires by HMMs within 24 h was confirmed by scanning electron microscopy/energy-dispersive X-ray spectrometry (SEM/EDX). In conclusion, ZnO nanowires are avidly ingested by HMMs and are highly cytotoxic, due to pH-triggered dissolution of the wires and intracellular ionic Zn^{2+} release. The induced cell death had features of both necrosis and apoptosis with severe ultrastructural changes to the mitochondria, suggesting that toxicity may be mediated by inhibition of cellular energy production.

METHODS

ZnO Template Synthesis. ZnO nanowires were fabricated by electrodeposition into a nuclear track-etch polycarbonate membrane. The rated membrane thickness, nominal pore size, and pore density were respectively 25 μm, 50 nm, and 6×10^8 pores/cm^2. One side of the polycarbonate membrane was first coated with a 100 nm thick layer of gold, by sputter deposition, to serve as a working electrode. The electrical contact was made to the membrane working electrode using a stainless steel plate. A platinum mesh was used as the counter electrode, and an Ag/AgCl (3 M KCl) electrode was used as the reference electrode. Electrodeposition was performed in electrolyte containing 0.1 M $Zn(NO_3)_2$ at a constant potential of −0.8 V *vs* Ag/AgCl at 65 °C. The reduction of nitrate ions in an aqueous solution serves as a source of hydroxide ion resulting in a pH-induced precipitation at the working electrode. The formation of ZnO follows the following mechanism:[42]

$$NO_3^- + H_2O + 2e^- \rightarrow NO_2^- + 2OH^-$$

$$Zn^{2+} + 2OH^- \rightarrow ZnO + H_2O$$

Liberation of ZnO Nanowires from Their Templates. ZnO nanowire templates (size ∼1−1.5 cm^2), complete with gold foil and polycarbonate polymer, were incubated in 2 mL DCM for ∼1 h to dissolve the polycarbonate template. After gently agitating the solution to dislodge the nanowires, the gold foil was removed with a pair of forceps. ZnO nanowires were collected by centrifugation at ∼2000 g, and the resulting pellet was washed six times with 2 mL of DCM to remove dissolved polycarbonate residue. Then, DCM was allowed to evaporate under a stream of nitrogen, and the resulting ZnO nanowires were suspended in pure ethanol. The concentration of ZnO nanowire stock solutions was determined using an Elan DRC^{Plus} inductively coupled plasma mass spectrometer (ICP-MS) (Perkin-Elmer Sciex, Beaconsfield, U.K.) *via* the measurement of ^{64}Zn, ^{66}Zn, and ^{68}Zn isotopes to establish total zinc concentration. These isotopes were selected as they exhibit a high natural abundance and therefore provided the most sensitive analysis. ZnO nanowire stock solutions were treated with 5% HNO_3 prior to analysis to ensure total ZnO dissolution. A standard additions approach was employed whereby unknown samples were spiked with a source of zinc nitrate (zinc calibration standard solution, 1000 mg/L, Fisher Scientific, Loughborough, U.K.) of incremented concentration. Unknown total zinc concentration was subsequently established following backward extrapolation of a series of spike calibration graphs.

Characterization of ZnO Nanowires. SEM of ZnO was performed with a Philips XL30 FEG-SEM operating at 5 kV using the secondary electron detector. Liberated ZnO nanowires were sputter coated with a 5 nm gold coating to prevent sample charging. TEM was performed with a Philips CM100 electron microscope operated at 80 kV. Nanowire dimensions were measured using ImageJ freeware (http://rsb.info.nih.gov/ij/). HR-TEM images were taken using a Titan electron microscope at 300 kV. Zn L2,3 edge jump ratio maps were acquired using a 40 eV energy slit using pre- and postedge energy windows centered at 995 ± 20 and 1040 ± 20 eV, respectively.

Isolation and Culture of Human Monocyte Macrophages. Mature human macrophages (HMMs) were obtained by *in vitro* culture of human monocytes isolated from human buffy coat residues (National Blood Service, Brentwood, U.K.), as described previously.[43] Briefly, monocytes were enriched by centrifugations on Ficoll and Percoll density gradients and seeded on tissue culture plates using macrophage serum-free medium (Mø-SFM; Invitrogen) supplemented with 100 U/mL penicillin and 100 μg/mL streptomycin. After incubation for 1 h at 37 °C, cells were washed twice with PBS to remove any remaining nonadherent cells, and monocytes were cultured at 37 °C in humidified air/5% CO_2 for at least 6−7 days prior to experiments, renewing the culture medium twice a week.

Neutral Red Assay. Following incubations, sample solutions were removed, and neutral red was added at a concentration of 40 μg/mL in Mø-SFM for 3 h at 37 °C in the dark. Then, cells were rinsed with PBS, and 500 μL extracting solution (50% ethanol, 1% glacial acetic acid) was added to each well. Plates were incubated for 15 min at room temperature in the dark to dissolve the dye, and 200 μL of dye extract was transferred to 96 well plates. Absorbance was measured at 570 nm using an ASYS HiTech Expert Plus plate reader, and cell viability was expressed in % based on a NA control.

Confocal Laser Fluorescence Microscopy. For live imaging, HMMs were cultured on 35 mm ø glass-based culture dishes (Iwaki, Japan) using Mø-SFM medium. Prior to imaging, cells were rinsed one time with warm imaging buffer (10 mM HEPES pH 7.4 containing 145 mM NaCl, 5 mM KCl, 1 mM $MgSO_4$, 1.5 mM $CaCl_2$, and 0.16% glucose) and loaded with 5 μM of the cell-permeant Zn^{2+}

indicator FluoZin3-AM (Invitrogen, U.K.) for 20 min at 37 °C (1 mL/insert in imaging buffer). After rinsing twice with warm imaging buffer, sample solutions were added in 2 mL imaging buffer containing 10 μg/mL PI (Sigma, U.K.). Live imaging was started immediately after addition of sample solutions using a Leica SP2 confocal laser microscope with an environmental chamber set to 37 °C. Imaging inserts were covered with a glass coverslip to avoid buffer evaporation. The 488 nm laser line was used to excite both FluoZin3-AM (ex 494 nm/em 516 nm) and PI (ex 535 nm/em 617 nm). The pinhole was set to ~5 AU to optimize image capture while minimizing irradiation damage to the live specimen. Images were acquired over a time period of ~5−6 h (1 frame/4 min) using a 20x objective (oil immersion, zoom 4). Fluorescence quantification (*f*/*f*0) was carried out using LCSLite Confocal Software (Leica, Germany).

ZnO Nanowire Dissolution in SBFs. The composition of SBFs was as follows: (1) ex-SBF pH 7.4, 25 mM HEPES−NaOH pH 7.4 containing 1 mM Na_2HPO_4, 2 mM $CaCl_2$, 1 mM $MgCl_2$, 5.8 mM KCl, 140.8 mM NaCl, and 5.6 mM glucose; (2) lyso-SBF pH 5.2, 25 mM MES−NaOH pH 5.2 containing 0.5 mM $CaCl_2$, 1 mM $MgCl_2$, and 200 mM KCl. ZnO nanowires (ZnO/7) liberated from their templates were incubated in 400 μL of ex- or lyso-SBF at 37 °C for 30 min. Two aliquots of 50 μL each were taken for the measurement of total Zn concentration. Undissolved ZnO nanowires were then removed by centrifugation for 10 min at room temperature (RT) in a table-top centrifuge using Vivaspin 500 filter inserts (3000 Da molecular weight cut off; Sartorius Stedim Biotech). Three aliquots of the filtrate were taken for the estimation of dissolved Zn concentration. Aliquots were diluted using 5% aqueous HNO_3 ensuring complete dissolution of ZnO for analysis by ICP-MS. DCM solvent controls were prepared in an analogous manner. Total Zn concentration was established *via* the measurement of all five stable isotopes of zinc (^{64}Zn, ^{66}Zn, ^{67}Zn, ^{68}Zn, and ^{70}Zn) using the ICP-MS instrumentation previously described. Being the most abundant, the ^{64}Zn, ^{66}Zn, and ^{68}Zn isotopes were used to establish zinc concentration of a lower concentration; the ^{67}Zn and ^{70}Zn isotopes were selected for measurement of high concentration. Zn quantification was undertaken *via* external calibration with a series of matrix-matched zinc nitrate standard solutions (as above) of the approximate range of 0.5−3000 μg L^{-1}. Analyte signal interference from ionic species of a similar mass-to-charge ratio to Zn was shown to be minimal by analysis of matrix-matched SBF blank solutions, and measurements were subsequently corrected by background subtraction.

Morphological dissolution of ZnO nanowires in SBFs of pH 5.2 and 7.4 was studied by TEM (ZnO/6). Five μL of ZnO/6 stock solution (in EtOH) was pipetted onto a 400 mesh holey carbon film grid and allowed to dry. Then, grids were submerged in 2 mL of SBFs at 37 °C for various lengths of time and quickly blotted dry using filter paper before viewing by TEM.

Sample Processing for TEM. For $ZnCl_2$ control experiments, HMMs were grown on six-well tissue culture plates. Following exposure to $ZnCl_2$, cells were washed in 0.9% saline and fixed in 4% glutaraldehyde/0.1 M PIPES buffer pH 7.2 for 1 h at 4 °C. After fixation, cells were scraped using a cell scraper and processed for TEM as described below in the form of a cell pellet. Due to the scarcity of the material, HMMs were grown on plastic-bottom culture inserts (Ibidi μ-dishes, Thistle Scientific, U.K.) for the ZnO experiments. Following exposures, cells were rinsed, fixed, as above, and then processed for TEM as monolayers *in situ* without scraping. Following fixation with glutaraldehyde, cells were rinsed several times in deionized water (DIW) to remove the fixative. Then, samples were osmicated (1% OsO_4, 0.15% potassium ferricyanide, and 2 mM $CaCl_2$ in DIW) for 1 h at RT. Again, the samples were washed several times with DIW and then bulk stained for 1 h at RT in the dark using uranyl acetate. Following two washes in DIW, the samples were dehydrated in graded solutions of ethanol (70, 95, and 100%), three times in each for 5 min, respectively. After two additional washes in 100% acetonitrile, the sample was infiltrated with Quetol 651 resin over four days using fresh resin each day. Resin was cured at 60 °C for 24 h. Ultrathin sections (~70 nm) of cell pellets or monolayers were cut using a Leica Ultracut E ultramicrotome and mounted on 300 mesh bare copper grids. In some cases, sections were post-stained for 2 min each in uranyl acetate and lead citrate and viewed using a Philips CM100 TEM operated at 80 kV. A multitude of cells were scanned by TEM to obtain a general impression of the sample, before images were taken.

Analysis of ZnO Nanowire Uptake by SEM/EDX. HMMs were grown on 10 mm ø Melinex coverslips (Agar Scientific) and incubated with 50 μg/mL ZnO nanowires (ZnO/4) for 1 h. Then, the cells were either processed for SEM immediately (0 h time point) or cultured on in the absence of nanowires for 4 h (4 h time point) or 24 h (24 h-point). Coverslips were quickly dipped twice in ice-cold distilled water, quench-frozen in propane cooled in liquid nitrogen, freeze-dried using an Edwards Auto 306 Turbo,[44] and carbon coated. SEM was carried out with a Philips XL-30 FEG-SEM. Images were taken with an accelerating voltage of 5 kV. EDX analysis was performed at 20 kV using an INCA x-sight analyzer and INCA software (Oxford Instruments).

Statistics. The significance of cytotoxicity experiments was calculated using Analyze-iT software embedded into ExCel using a one-way ANOVA followed by a least significant difference (LSD) posthoc test. Differences of $p \leq 0.01$ were chosen as significant.

Acknowledgment. This project and K. Müller were funded by KAUST (King Abdullah University of Science and Technology).

Supporting Information Available: Figure S1 contains three confocal live imaging movies showing the rise of intracellular, free Zn^{2+} in HMMs prior to cell death. This material is available free of charge *via* the Internet at http://pubs.acs.org.

REFERENCES AND NOTES

1. Zhou, J.; Xu, N.; Wang, Z. L. Dissolving Behaviour and Stability of ZnO Wires in Biofluids: a Study on Biodegradability and Biocompatibility of ZnO Nanostructures. *Adv. Mater.* **2006**, *18*, 2432–2435.
2. Wang, L. W.; Song, J. Piezoelectric Nanogenerators Based on Zinc Oxide Nanowire Arrays. *Science* **2006**, *312*, 242–246.
3. Wang, Z. L. Splendid One-Dimensional Nanostructures of Zinc Oxide: a New Nanomaterial Family for Nanotechnology. *ACS Nano* **2008**, *2*, 1987–1992.
4. Vallee, B. L.; Falchuk, K. H. The Biochemical Basis of Zinc Physiology. *Physiol. Rev.* **1993**, *73*, 79–118.
5. Stefanidou, M.; Maravelias, C.; Dona, A.; Spiliopoulou, C. Zinc: A Multipurpose Trace Element. *Arch. Toxicol.* **2006**, *80*, 1–9.
6. Overbeck, S.; Rink, L.; Haase, H. Modulating the Immune Response by Oral Zinc Supplementation: A Single Approach for Multiple Disorders. *Arch. Immunol. Ther. Exp.* **2008**, *56*, 15–30.
7. Prasad, A. S. Zinc in Human Health: Effect of Zinc on Immune Cells. *Mol. Med.* **2008**, *14*, 353–357.
8. Lansdown, A. B. G.; Mirastschijiski, U.; Stubbs, N.; Scanlon, E.; Agren, M. S. Zinc in Wound Healing: Theoretical, Experimental and Clinical Aspects. *Wound Repair Regen.* **2007**, *15*, 2–16.
9. Newman, M. D.; Stotland, M.; Ellis, J. I. The Safety of Nanosized Particles in Titanium Dioxide - and Zinc Oxide-Based Sunscreens. *J. Am. Acad. Dermatol.* **2009**, *61*, 685–692.
10. Gordon, T.; Fine, J. M. Metal Fume Fever. *Occup. Med.* **1993**, *8*, 504–517.
11. Cuajungco, M. P.; Faget, K. Y. Zinc Takes the Center Stage: Its Paradoxical Role in Alzheimer's Disease. *Brain Res. Brain Res. Rev.* **2003**, *41*, 44–56.
12. Bitanihirwe, B.; Cunningham, M. Zinc: The Brain's Dark Horse. *Synapse* **2009**, *63*, 1029–1049.
13. Sensi, S. L.; Paoletti, P.; Bush, A. I.; Sekler, I. Zinc in the Physiology and Pathology of the CNS. *Nature Rev.* **2009**, *10*, 780–792.
14. Gulson, B.; McCall, M.; Korsch, M.; Gomez, L.; Casey, P.; Oytam, Y.; Taylor, A.; Kinsley, L.; Greenoak, G. Small Amounts of Zinc from Zinc Oxide Particles in Sunscreens Applied Outdoors Are Absorbed Through Human Skin. *Toxicol. Sci.* **2010**, epub ahead of print.

15. Kahru, A.; Dubourguier, H. C. From Ecotoxicology to Nanoecotoxicology. *Toxicology* **2010**, *269*, 105–119.
16. Blinova, I.; Ivask, A.; Heinlaan, M.; Mortimer, M.; Kahru, A. Ecotoxicity of Nanoparticles of CuO and ZnO in Natural Water. *Environ. Pollut.* **2010**, *158*, 41–47.
17. Wong, S. W.; Leung, P. T.; Djurisic, A. B.; Leung, K. M. Toxicities of Nano Zinc Oxide to Five Marine Organisms: Influences of Aggregate Size and Ion Solubility. *Anal. Bioanal. Chem.* **2010**, *396*, 609–618.
18. Xia, T.; Kovochich, M.; Liong, M.; Madler, L.; Gilbert, G.; Shi, H.; Yeh, J. I.; Zink, J. I.; Nel, A. E. Comparison of the Mechanism of Toxicity of Zinc Oxide and Cerium Oxide Nanoparticles Based on Dissolution and Oxidative Stress Properties. *ACS Nano* **2008**, *2*, 2121–2134.
19. Yang, H.; Liu, C.; Yang, D.; Zhang, H.; Xi, Z. Comparative Study of Cytotoxicity, Oxidative Stress and Genotoxicity Induced by four Typical Nanomaterials: The Role of Particle Size, Shape and Composition. *J. Appl. Toxicol.* **2009**, *29*, 69–78.
20. Deng, X.; Luan, Q.; Chen, W.; Wang, Y.; Wu, M.; Zhang, H.; Jiao, Z. Nanosized Zinc Oxide Particles Induce Neural Stem Cell Apoptosis. *Nanotechnology* **2009**, *20*, 115101.
21. Goux, A.; Pauporte, T.; Chivot, J.; Lincot, D. Temperature Effects on ZnO Electrodeposition. *Electrochim. Acta* **2005**, *50*, 2239–2248.
22. Vayssieres, L.; Keis, K.; Hagfeldt, A.; Lindquist, S.-E. Three-Dimensional Array of Highly Oriented Crystalline ZnO Microtubes. *Chem. Mater.* **2001**, *13*, 4395–4398.
23. Illy, B. Electrodeposition of Zinc Oxide Nanostructured Films. Ph.D. Thesis, Imperial College London, London, U.K., 2009.
24. Gojova, A.; Guo, B.; Kota, R. S.; Rutledge, J. C.; Kennedy, I. M.; Barakat, A. I. Induction of Inflammation in Vascular Endothelial Cells by Metal Oxide Nanoparticles: Effect of Particle Composition. *Environ. Health Perspect.* **2007**, *115*, 403–409.
25. Lin, W.; Xu, Y.; Huang, C. C.; Ma, Y.; Shannon, K. B.; Chen, D. R.; Huang, Y. W. Toxicity of Nano- and Micro-Sized ZnO Particles in Human Lung Epithelial Cells. *J. Nanopart. Res.* **2009**, *11*, 25–39.
26. Lee, J.; Kang, B. S.; Hicks, B.; Chancellor, T. F.; Chu, B. H.; Want, H. T.; Keselowsky, B. G.; Ren, F.; Lele, T. The Control of Cell Adhesion and Viability by Zinc Oxide Nanorods. *Biomaterials* **2008**, *29*, 3743–3749.
27. Zaveri, T. D.; Dolgova, N. V.; Chu, B. H.; Lee, J.; Wong, J.; Lele, T. P.; Ren, F.; Keselowsky, B. G. Contributions of Surface Topography and Cytotoxicity to the Macrophage Response to Zinc Oxide Nanorods. *Biomaterials* **2010**, *31*, 2999–3007.
28. Kroll, A.; Pillukat, M. H.; Hahn, D.; Schnekenberger, J. Current *In Vitro* Methods in Nanoparticle Risk Assessment: Limitations and Challenges. *Eur. J. Pharmaceut. Biopharmaceut.* **2009**, *72*, 370–377.
29. Zhang, Y.; Muhammed, M. Critical Evaluation of Thermodynamics of Complex Formation of Metal Ions in Aqueous Solutions IV. Hydrolysis and Hydroxo-Complexes of Zn^{2+} at 298.15 K. *Hydrometallurgy* **2001**, *60*, 215–236.
30. Deng, Z. J.; Mortimer, G.; Schiller, T.; Musumeci, A.; Martin, D.; Minchin, R. F. Differential Plasma Protein Binding to Metal Oxide Nanoparticles. *Nanotechnology* **2009**, *20*, 455101.
31. Wester, K.; Asplund, A.; Backvall, H.; Micke, P.; Derveniece, A.; Hartmane, I.; Malstrom, P.-U.; Ponten, F. Zinc-Based Fixative Improves Preservation of Genomic DNA and Protein in Histoprocessing of Human Tissues. *Lab. Invest.* **2003**, *83*, 889–899.
32. Formigari, A.; Irato, P.; Santon, A. Zinc, Antioxidant Systems and Metallothionein in Metal Mediated-Apoptosis: Biochemical and Cytochemical Aspects. *Comp. Biochem. Physiol., Part C: Toxicol. Pharmacol.* **2007**, *146*, 443–459.
33. Lee, J. Y.; Hwang, J. J.; Park, M. H.; Koh, J. Y. Cytosolic Labile Zinc: A Marker for Apoptosis in the Developing Rat Brain. *Eur. J. Neurosci.* **2006**, *23*, 4435–4442.
34. Sensi, S. L.; Zin, H. Z.; Weiss, J. H. AMPA/Kainate Receptor-Triggered Zn^{2+} Entry into Cortical Neurons Induces Mitochondrial Zn^{2+} Uptake and Persistent Mitochondrial Dysfunction. *Eur. J. Neurosci.* **2000**, *12*, 3813–3118.
35. Dineley, K. E.; Votyakova, T. V.; Reynolds, I. J. Zinc Inhibition of Cellular Energy Production: Implications for Mitochondria and Neurodegeneration. *J. Neurochem.* **2003**, *85*, 563–570.
36. Sharma, V.; Shukla, R. K.; Saxena, N.; Parmar, D.; Das, M.; Dhawan, A. DNA Damaging Potential of Zinc Oxide Nanoparticles in Human Epidermal Cells. *Toxicol. Lett.* **2009**, *185*, 211–218.
37. George, S.; Pokhrel, S.; Xia, T.; Gilbert, B.; Ji, Z.; Schowalter, M.; Rosenauer, A.; Damoiseaux, R.; Bradley, K. A.; Mädler, L. Use of a Rapid Cytotoxicity Screening Approach to Engineer a Safer Zinc Oxide Nanoparticle Through Iron Doping. *ACS Nano* **2010**, *4*, 15–29.
38. Horie, M.; Nishio, K.; Fujita, K.; Endoh, S.; Miyauchi, A.; Saito, Y.; Iwahashi, H.; Yamamoto, K.; Murayama, H.; Nakano, H.; et al. Protein Adsorption of Ultrafine Metal Oxide and Its Influence on Cytotoxicity Toward Cultured Cells. *Chem. Res. Toxicol.* **2009**, *22*, 543–553.
39. Brayner, R.; Dahoumane, S. A.; Yepremian, C.; Djediat, C.; Meyer, M.; Coute, A.; Fievet, F. ZnO Nanoparticles: Synthesis, Characterization and Ecotoxicological Studies. *Langmuir* **2010**, *26*, 6522–6528.
40. Zhang, B.; Kong, T.; Xu, W.; Su, R.; Gao, Y.; Cheng, G. Surface Functionalization of Zinc Oxide by Carboxyalkylphosphonic Acid Self-Assembled Monolayers. *Langmuir* **2010**, *26*, 4514–4522.
41. Zinc, Health Professional Fact Sheet; National Institutes of Health; Office of Dietary Supplements: Bethesda, MD, 2009; http://ods.od.nih.gov/factsheets/zinc.asp.
42. Ingham, B.; Illy, B. N.; Ryan, M. P. Direct Observation of Distinct Nucleation and Growth Processes in Electrochemically Deposited ZnO Nanostructures Using *In Situ* XANES. *Phys. Chem. C* **2008**, *112*, 2820–2824.
43. Müller, K.; Skepper, J. N.; Posfai, M.; Trivedi, R.; Howarth, S.; Corot, C.; Lancelot, E.; Thompson, P. W.; Brown, A. P.; Gillard, J. H. Effect of Ultrasmall Superparamagnetic Iron Oxide Nanoparticles (Ferumoxtran-10) on Human Monocyte-Macrophagas *In Vitro*. *Biomaterials* **2007**, *28*, 1629–1642.
44. Warley, A.; Skepper, J. N. Long Freeze-Drying Times Are Not Necessary During the Preparation of Thin Sections for X-Ray Microanalysis. *J. Microsc.* **2000**, *198*, 116–123.